Computational and Theoretical Chemistry 1072 (2015) 43–51

Contents lists available at ScienceDirect

Computational and Theoretical Chemistry

journal homepage: www.elsevier.com/locate/comptc

Lithium migration at low concentration in TiO_2 polymorphs

Corinne Arrouvel [a,b,c,*], Thiago C. Peixoto [b,d], Mario E.G. Valerio [b], Stephen C. Parker [a]

[a] University of Bath, Department of Chemistry, Bath BA2 7AY, UK
[b] Universidade Federal de Sergipe, Departamento de Física, São Cristóvão, Sergipe 49100-000, Brazil
[c] Universidade Federal de São Carlos, DFQM, Sorocaba, SP 18052-780, Brazil
[d] Universidade Estadual Paulista, Instituto de Física Teórica, São Paulo, SP 01140-070, Brazil

ARTICLE INFO

Article history:
Received 22 July 2015
Received in revised form 2 September 2015
Accepted 2 September 2015
Available online 7 September 2015

Keywords:
Lithium-ion batteries
Anode
Atomistic simulations
3D pathways
TiO_2-B
Anatase

ABSTRACT

We report an atomistic simulation study at low concentration of lithium in scanning all the possible pathways for Li migration in TiO_2 polymorphs. We are particularly interested in showing the effects of the structural properties on the intercalation energies and on the energy barriers for ion diffusion. The most favourable directions for Li^+ transport are highlighted and we observe an anisotropic diffusion in rutile, brookite and TiO_2-B whereas the diffusion is isotropic in the case of anatase. The lowest energy barrier is calculated in rutile but it is not a key factor to determine the efficiency of Li-battery materials. Intercalation energies of stable and transition states are however important data to take into account as well as the Li pathway in order to evaluate the potentiality of each polymorph for Li migration.

1. Introduction

The migration of extrinsic and intrinsic defects plays a key role in many industrial applications such as lithium-ion batteries and fuel cells. However, understanding the mechanism of the intercalation and diffusion at the atomic scale is often not well understood.

Recent reviews and theoretical work [1–6] have been devoted to anode and cathode electrodes. Titanium oxides are very promising anode materials and particularly the TiO_2-B phase. TiO_2-B shows a higher capacity [7–9] (up to 338 mA h/g on nanotubes [8] and more recently up to 360 mA h/g on nanoribbons [10]) than the other polymorphs. This phase is less dense than rutile, anatase and brookite phases (respectively 3.73–3.75 g/cm^3 [11,12], 4.26 g/cm^3 [13], 3.92 g/cm^3 [13], 4.12 g/cm^3 [14]) which can explain its efficiency for Li-batteries. Also, there are numerous theoretical and experimental studies on the intercalation of lithium in rutile and anatase [15–33], there is an increasing number of studies on TiO_2-B [3–7,23,32,34–38], few studies on other phases of titania [39–43], rarer on brookite [6,44–48] and scarce on amorphous TiO_2 [49,50]. Like the rutile, the brookite phase has shown no attractiveness for Li-battery unless we reach the nanoparticle size. Only small nanoparticles allow to intercalate a decent quantity of lithium (up to 0.95 Li/Ti in brookite [44], up to 0.85 Li/Ti in rutile [51]) and phase transformations are frequently observed in the case of anatase and rutile [51–53]. The migration of Li is another important point to understand. The ionic diffusion coefficients are difficult to obtain experimentally and a wide range of values has been reported due to the fact that the diffusion can be calculated microscopically or macroscopically. For example, on the anatase phase, various values on the Li diffusion coefficient can be found in the literature, from 10^{-12} to 10^{-17} cm^2/s [26,54]. Other phenomena influence the diffusion coefficient such as the temperature (the coefficient increases as the temperature increases) and the phase transformation (anatase transforms reversibly to an Li-titanate phase around Li/Ti $\sim$ 0.5 and the coefficient decreases [26,30]). The highest Li diffusion coefficient has been experimentally measured for the rutile phase [55] (anisotropic diffusion of 2.7×10^{-3} cm^2/s along the *c* direction with an activation energy of 0.3 eV) at the meantime, the main obstacle is to intercalate Li in large particle sizes [51]. The activation energy in the case of TiO_2-B is about 0.48 eV [56].

We use empirical methods to give new insights on the Li migration through a systematic study. The specific purpose of this work is to detail the diffusion pathways, intercalation sites and to explain the potentiality of Li-battery materials through their energetic and structural properties.

* Corresponding author at: Universidade Federal de São Carlos, DFQM, Sorocaba, SP 18052-780, Brazil.
E-mail address: corinne@ufscar.br (C. Arrouvel).

http://dx.doi.org/10.1016/j.comptc.2015.09.002
2210-271X/

2. Methods

The atomistic simulations are undertaken using METADISE [57] (Minimum Energy Techniques Applied to Dislocation, Interface, and Surface Energies) and GULP [58,59] (General Utility Lattice Program). METADISE has been mainly used to scan the different pathways in TiO_2 polymorphs and GULP is used to refine the punctual defect calculations.

2.1. Interatomic potential methods

The simulations with METADISE and GULP are based on a Born model of solid assuming that the ions interact via long-range electrostatic forces (Coulombic interactions) and short-range forces including both the repulsions and the van der Waals attractions between neighbouring electron charge clouds [60]. In this study, different potentials have been tested and we have opted for interatomic potentials from Kerisit et al. [6] with a core–shell model which was derived from Matsui and Akoagi (MA) potentials [61] for TiO_2. $LiTiO_2$ potentials have been further tested and compared to previous DFT calculations on TiO_2-B [3,4] and experimental data [36].

The potentials follow the relation:

$$V_{r_{ij}} = \sum \frac{q_i q_j}{r_{ij}} + A_{ij}\exp(-r_{ij}/\rho_{ij}) - \frac{C_{ij}}{r_{ij}^6}$$

With r_{ij} the separation between the ions i and j; q_i and q_j the charges of each ion acting in the Coulombic term; and A_{ij}, ρ_{ij}, C_{ij} the ion–ion parameters in the Buckingham relation.

2.2. Scan of Li pathways

One of the strengths of using interatomic potential models is that the total energy of the system can be evaluated rapidly. Thus we are able to exploit this by performing a simple scan of the total interaction energy as a function of the lithium position. This is achieved by simply adjusting the position of the lithium ion in steps of 0.1 Å within the unit cell, and then calculating the energy. As we use the shell model, after each update of the lithium position we allow the shells to relax and hence this mimics to a limited extent electronic relaxation and provides an approximate representation of the polarisation of the crystal as the lithium is moved through the lattice. The energies are calculated using the METADISE [57] code and the energy profile and the isosurfaces are plotted using VESTA [62].

2.3. Defect calculations

GULP uses the Mott–Littleton approach [63], which is also a two-regions approach. The region I is around the defect (Li^+ intercalation in our case) and is allowed to fully relax. The region II surrounding the region I is fixed and represents the rest of the crystal involving quasi-continuum methods. The sizes of the two regions are 14 Å (region I) and 22 Å (region II).

We note that the defect calculation is referred to the intercalation of the Li^+ in the gas phase, therefore this value can be directly compared to the voltage, or intercalation of Li metal. However, the relative energies between defect calculations should follow the same trend at low concentration if we consider that the energetic process to transform Li metal in Li gas, to oxidise Li into Li^+ and to reduce the Ti network is the same for all the polymorphs.

3. Results

3.1. Bulk crystal structures of TiO_2 polymorphs

The bulk crystal structures of rutile [64], anatase [65], brookite [66] and TiO_2-B [11] obtained from X-ray data are summarised in Table 1. Most of TiO_2 polymorphs have Ti species with a coordination number of 6 and O species with a coordination of 3. The exception is for TiO_2-B which has O ions with different coordination numbers of 2, 3 and 4.

The bulk crystal structure of the polymorphs has already been calculated and well detailed by Kerisit et al. [6]. To better understand the Li intercalation and diffusion, we summarise few key energetic and structural characteristics in Table 2. The stability order using minimisation techniques with Kerisit et al.'s potential is as follows:

Rutile > Brookite > Anatase > TiO_2-B

The density and the average of Ti–O distances follow the same order, the rutile phase being the densest and getting the shortest average Ti–O distances. The TiO_2-B phase is interesting for Li-ion batteries, being the less dense of those polymorphs and having a higher experimental capacity. The range of distances is wider; this phase gets the shortest and the longest Ti–O distances. The shortest Ti–O distances are linked to the 2-fold oxygen (about 1.84 Å) and a relatively wide infinite channel is between the 2-fold oxygens. Another channel is visible along the c direction of TiO_2-B. In the case of the rutile phase, a channel can be observed along the c direction but due to the denser structure, the channel is thinner.

3.2. Pathways for Li migration

The energy profiles for each polymorph obtained with METADISE are shown in Fig. 1 and the most stable channels for the Li diffusion are represented. The centre of the channels, where the

Table 1
Structural characteristics of experimental TiO_2 polymorphs.

	Rutile [64]	Anatase [65]	Brookite [66]	TiO_2-B [11]
Space group (number)	$P4_2/mnm$ (136)	$I\,4_1/amd$ (141)	Pbca (61)	C2/m (12)
Crystal system	Tetragonal	Tetragonal	Orthorhombic	Monoclinic
a (Å)	4.60	3.78	9.18	12.18
b (Å)	4.60	3.78	5.45	3.74
c (Å)	2.96	9.51	5.14	6.52
Cell volume (Å^3)	62.61	136.26	257.38	284.22
Density (g/cm^3)	4.24	3.89	4.12	3.73
Number of TiO_2 units, Z	2	4	8	8
Ti–O distance range	1.97 * 2 1.96 * 4	1.98 * 2 1.93 * 4	1.99 1.87 1.99 1.92 1.94 2.04	1.81–2.26

Table 2
Structural characteristics of calculated TiO_2 polymorphs using Kerisit et al.'s potential.

	Rutile	Anatase	Brookite	TiO_2-B
Lattice energy (eV)	−39.807	−39.521	−39.642	−39.345
[a] a (Å)	4.499	3.782	9.138	12.273
[a] b (Å)	4.499	3.782	5.399	3.761
[a] c (Å)	3.002	9.470	5.131	6.463
[b] V (Å[c])	60.751	135.494	253.141	286.202
[c] d (g/cm[c])	4.367	3.916	4.192	3.708
[d] $D_{(Ti-O)}$ (Å)	(2) 1.921	(4) 1.926	1.916	1.836
	(4) 1.960	(2) 2.002	1.922	1.900
			1.930	(2) 1.952
			1.953	2.003
			1.982	2.141
			1.999	
[e] $R_{(Ti-O)}$ (Å)	0.038	0.076	0.082	0.305
[f] $\overline{D}_{(Ti-O)}$ (Å)	1.947	1.952	1.950	1.964

[a] Crystalline parameters.
[b] Unit cell volume.
[c] Density.
[d] Ti–O distances.
[e] Ti–O distance range.
[f] Ti–O average distances.

colours tend to the red, is the most stable region. We define the C site being a stable site, usually at the intersection of pathways.

3.2.1. Rutile

In Fig. 1a, we can observe that the wider channel is along the [0 0 1] direction. The Li diffusion is predicted to be more favourable and linear, in 1 dimension. Another direction of diffusion is visible, along the plane (a, b). The path at height $c = 0$ is in zigzag along the [1 1 0] direction and the path at height $c = 0.5$ is along the [$\bar{1}$ 1 0] direction. Therefore, we consider the second pathway in 2D.

The C centre is then at the intersection of the channels [0 0 1] and [1 1 0]. From the geometrical point of view, we can define the C site being with a symmetry D_{4h}.

3.2.2. Anatase

The pathway for Li diffusion is in zigzag within the 3 directions in the space (see Fig. 1b). The symmetry of the C site is Td (Tetrahedral). The Li can diffuse along a combination of [2 0 1] directions and their equivalent (i.e. [2 0 1] = [0 2 1] = [$\bar{2}$ 0 1] = [0 $\bar{2}$ 1]).

3.2.3. Brookite

In the case of the brookite phase, the pathway is more complex, in zigzag and more diffuse. We can observe pairs of channels along the c direction. A pair of channels is linked by a segment in a direction quasi-perpendicular. Therefore, the diffusion is expected to be along the c-direction, along each pair of channels. The C-site has a C_1 symmetry.

We note that the second route along (a, b) direction, which should connect pair of channels, is not favourable. Then we consider that the unique possible way if Li diffusion within the bulk will be along the c direction.

3.2.4. TiO_2-B

This polymorph gets the widest diffusion profiles and a wide stable region around the C site. The most favourable pathway is along the [0 1 0] direction. Another route is visible along the c direction. It appears from the energy profile that this second pathway is in zigzag.

If we consider the C site (at the fractional coordinates 0.0 0.5 0.0), it is surrounded by 8 oxygen atoms and its symmetry is D_{2h}. The C site is not the most stable site but the Li ion relaxes in an off-centre position. We will detail more explicitly about this stable site in Section 3.3.4.

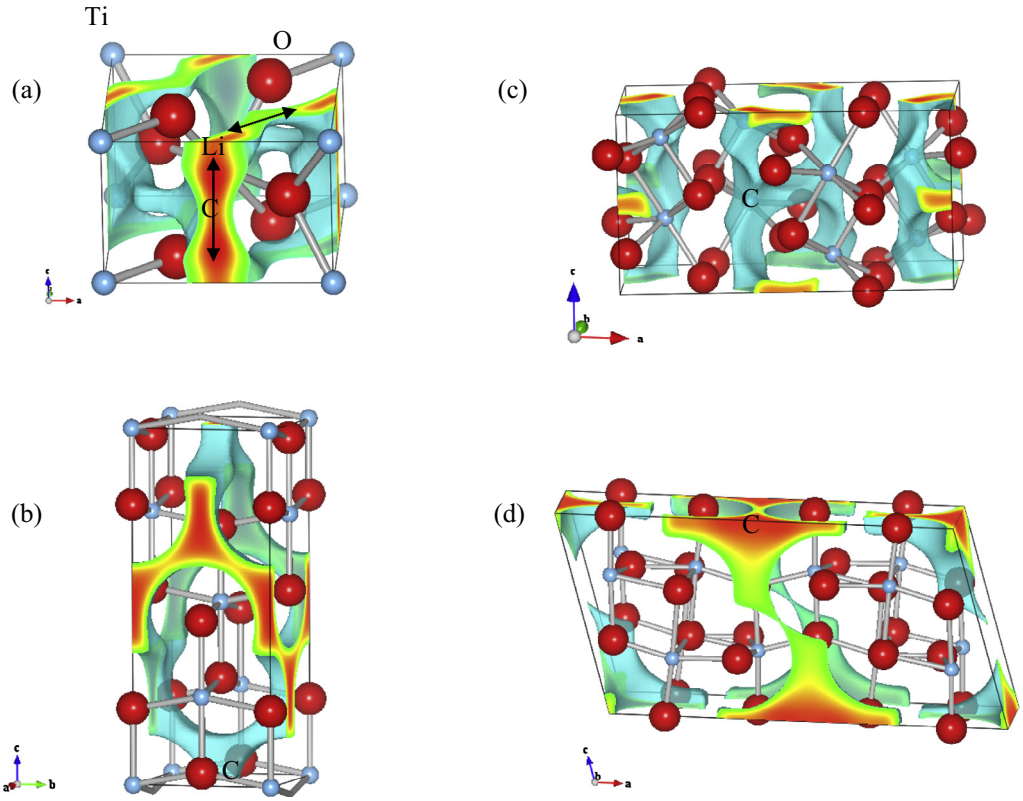

Fig. 1. Pathways of Li migration in (a) rutile; (b) anatase; (c) brookite; (d) TiO_2-B (Regions in red correspond to the Li^+ diffusion with the lowest intercalation energy). (For interpretation of the references to colour in this figure legend, the reader is referred to the web version of this article.)

3.2.5. Amorphous TiO_2

There are various methods to synthetize high-density/low density amorphous TiO_2 [49,67–72] and pressure-induced amorphization method enables to obtain low density amorphous phase [71]. The choice of our density is based on experimental data in order to get it in the same range of anatase and TiO_2-B.

An amorphous phase of 60 TiO_2 units in the periodic cell with a density of 3.8 g/cm^3 has been generated with a stochastic quenching procedure and firstly optimised using the same *ab initio* methods as described in Lizárraga et al.'s article [73]. Density Functional Theory (DFT) calculations have been done using VASP code [74], with GGA-PW91 [75] functional and PAW method [76]. The convergence on electronic and geometric (using a conjugate gradient algorithm) criterions are respectively 0.1 meV and 1 meV, a cutoff on the kinetic energy is of 250 eV and a k-point grid is at the gamma point. The optimised DFT structure is re-optimised with METADISE and some further analysis has been undertaken in order to verify the validity of our model, using the same procedure as in Lizárraga et al.'s study [73] for the radial distribution function (RDF), bond lengths and coordination number calculations (with a cutoff on Ti–O bond distances of 2.6 Å).

The structure analysis shows reasonable agreement with previous experimental [68,72] and theoretical studies [77–82] and some small differences can come from the density of the models as it has been demonstrated in similar comparative studies [73,82]. From the total pair-radial distribution function $g(r)$, the first peak corresponding to Ti–O distances is 1.93 Å and the second peak O–O is at 2.59 Å for our model with a density of 3.8 g/cm^3. The average on Ti coordination number is 5.6 with mainly fivefold Ti and 6-fold Ti, some 4-fold Ti are observed with the cutoff of 2.6 Å on the distance criterion. If a cutoff of 3.0 Å is considered, the 4-fold species are not observed anymore.

The results on amorphous phase are not detailed in the present paper but it supports the utility and consistency of using METADISE as a preliminary study which can be further extended.

3.3. Li intercalation sites

From the energy profile, the most stable and transition sites have been optimised at constant pressure using GULP and as well some intermediary sites between the minima and maxima. Table 3 resumes the energetic and structural properties of the main sites. The C site, defined previously, is in fact the most stable site. We report the hopping distance between C sites and the activation energy is the energy difference between the most stable site (C site) and the transition site T[hkl] for each [hkl] possible direction. Lithium site characteristics for each polymorph are detailed as follows and the impact of the geometry on the intercalation sites and then on energy barriers are discussed in Section 4.

3.3.1. Rutile

From the energy profile, we have identified two paths from the C site, being the most stable site with an intercalation energy of −1.60 eV (Fig. 2a). The first path is along the *c* direction, the barrier is denoted by T[0 0 1] with an intercalation energy of −1.56 eV. The barrier is a tetrahedral site, Td, with average Li–O distances of 1.83 Å. Outside the tetrahedron, we report a second Td site (second neighbours) with longer Li–O distances, at 2.71 Å. The second path is along the [1 1 0] direction, the site at the barrier (E_{int} = +0.31 eV) is a deformed Td with two Li–O distances at 1.82 Å and two Li–O distances at 1.72 Å. The average of Li–O distances is 1.77 Å, shorter distances compared to T[0 0 1] site. The 2nd neighbours get also slightly shortest distances at 2.67 Å. A fast diffusion is therefore expected along the *c* direction whereas the diffusion is unfavourable along the [1 1 0] direction.

3.3.2. Anatase

The C site in anatase is in an octahedral environment, Oh. The basal plan is not planar and the symmetry of the site is then C_{2v}. The C site, with average Li–O bond distances of 2.16 Å and with an intercalation energy of −2.20 eV, is not the most stable one. The Li is displaced up or down along the C_2 rotation axis and its coordination number changes from 6-fold to 5-fold with an average shortening of the distances, at 1.99 Å. The off-centre site is a distorted Oh site, stabilizing slightly the energy, E_{int} = −2.21 eV (Fig. 2b).

From the C site, the lithium can move to four equivalent [2 0 1] directions. The T[2 0 1] site is in an Oh environment with a planar basal plan. The average of Li–O distances is 2.06 Å and the symme-

Table 3
Intercalation sites (in bold, lowest intercalation energy for each polymorph).

Polymorph	Fractional coordinates	Wyckoff notation	$E_{int.}$ (eV)	Li coordination	Li symmetry	$\overline{D}$ Li–O (Å)
Rutile	(C)[a] 0.5 0.0 0.5	4c	**−1.60**	6	D_{4h}	1.99
	T[0 0 1][c] 0.5 0.0 0.25	4d	−1.56	4	Td	1.83
	T[1 1 0][c] 0.7 0.3 0.0	4g	0.31	4	Td[d]	1.77
Anatase	(off-C)[b] 0.5 0.5 0.0364	16f	**−2.21**	5	C_{2v}	1.99
	(C)[a] 0.5 0.5 0.0	4b	−2.20	6	C_{2v}	2.16
	(T[0 $\bar{2}$ 1][c] 0.5 0.25 0.125	8d	−1.79	6	D_{4h}	2.06
Brookite	(C)[a] 0.59 0.61 0.54	8c	**−2.13**	6	Oh[d]	2.07
	(T[0 0 1])[c] 0.59 0.67 0.87	8c	−1.06	4	Td[d]	1.82
	(M) 0.5 0.5 0.5	4b	−1.94	6	Oh[d]	2.02
TiO_2-B	(off-C)[b] 0.0 0.4 0.0	4g	**−2.60**	4 (6)[e]	C_{2v}	2.35 (2.51)[e]
	(C)[a] 0.0 0.5 0.0	2b	−2.59	4	D_{4h}	2.30
	A1 0.062 0.5 0.341	4i	−1.96	5	σ_v (C_{2v}[d])	2.04
	A2 0.12 0.5 0.0	4i	−2.39	5	σ_v (C_{2v}[d])	2.07
	T[1 0 0] 0.25 0.25 0.0	4e	−1.51	6	Oh	2.13
	T[0 1 0] 0.0 0.0 0.0	2a	−2.07	4	D_{2h}	2.00
	T[0 0 1] 0.0 0.5 0.5	2d	−1.63	6	Oh	2.05

[a] Stable C site.
[b] Off-centre C site.
[c] T: Transition site.
[d] Deformed.
[e] Including second-order O ions.

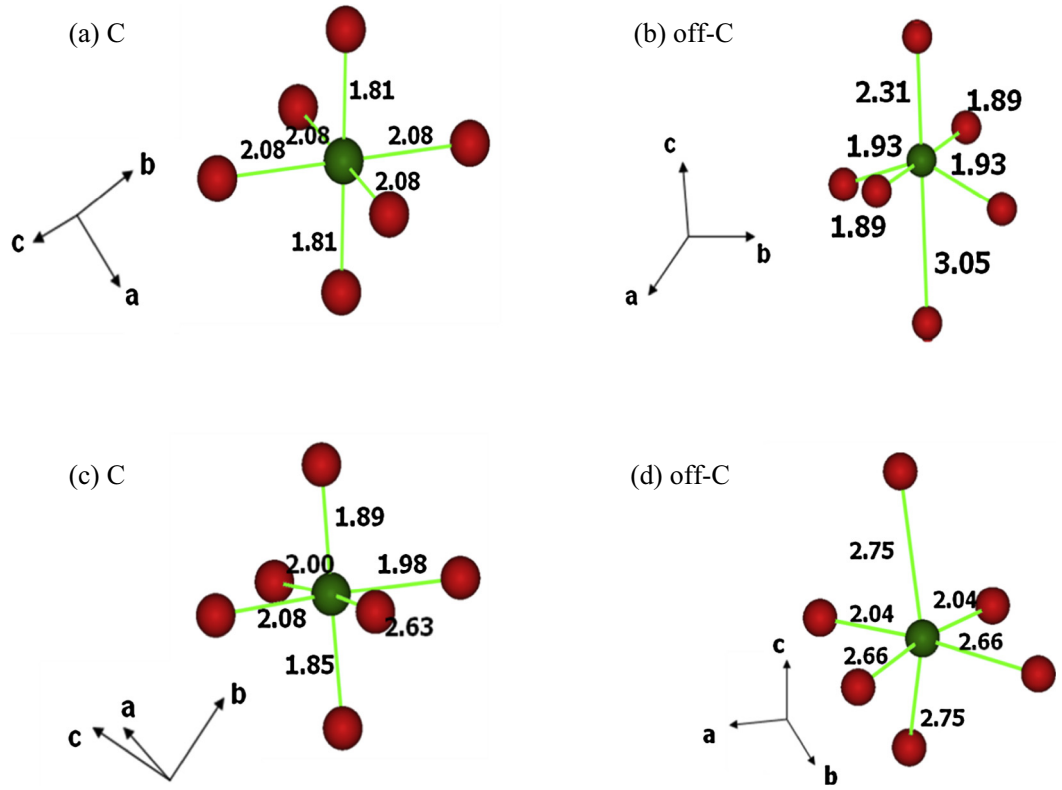

Fig. 2. Li environment for each most stable site in (a) rutile; (b) anatase; (c) brookite; (d) TiO_2-B (Li–O distances in Angströms).

try is D_{4h}. The site is particularly stable, with an intercalation energy of −1.79 eV.

3.3.3. Brookite

We saw previously that the path is along the *c* direction with a possible cross between two channels. The C site (Fig. 2c) is the most stable site in a pseudo-octahedral environment, with Li–O distances of 2.07 Å and its symmetry is C_1. Its intercalation energy is about −2.13 eV. The site in the middle of two juxtaposed channels is called M site. The M site is also stable, −1.94 eV with an average Li–O distance of 1.82 Å, being as well a distorted Oh site. The transition site T[001] is however in a distorted tetrahedral environment, with Li–O distances of 1.82 Å and E_{int} of −1.06 eV.

3.3.4. TiO_2-B

For TiO_2-B, due to its more complex structure, several stable sites and three possible directions for the Li diffusion are reported. The C site (E_{int} = −2.59 eV) is in the square-planar of D_{4h} symmetry if we consider only the four shortest Li–O distances at 2.30 Å. The volume of this site is the widest but the off-centre C-site is favoured (with E_{int} = −2.60 eV). The Li is shifted along the *b* direction, becoming the C_2 rotation axis. The symmetry of this site is then C_{2v} (Fig. 2d). The coordination is 4-fold with an average Li–O distance of 2.35 Å when we consider that the oxygen atoms out-of-plane are second range neighbours. The differentiation between the first-order and the second-order neighbours is not obvious and the relaxed site can also be considered in a pseudo-octahedral environment if we include the second-order O ions with longer Li–O distances of 2.75 Å. In the latter case, the average of distances is 2.51 Å and the site is considered 6-fold. Those large distances can explain why the energy profile on the Li diffusion around the C site is so wide. At the proximity of the C site, the intercalation energy is also low which can result in the difficulty to experimentally measure the position of the C site by XRD. The second most stable site is the A2 site (E_{int} = −2.39 eV), which is in agreement with previous DFT studies [4]. The site is 5-fold with Li–O distances of 2.07 Å. The third stable site is the A1 site, also 5-fold with an intercalation energy of −1.96 eV. In this case, we did fix the position of Li at the fractional coordinates 0.0624 0.5000 0.3414 to avoid the spontaneous relaxation towards the C site (as the c component of A1 site decreases, the intercalation energy increases). The average Li–O distance is 2.04 Å.

If we look at the diffusion from the C site, there are three inequivalent path directions along *a*, *b*, *c* axis corresponding respectively to the barrier sites T[100], T[010] and T[001]. The path along the a direction is in zigzag and it is the less favourable path, the T[100] site having an intercalation energy of −1.51 eV, corresponding to an energy barrier of 1.09 eV. The Li is in an octahedral environment, with an average Li–O distance of 2.13 Å. The path along the *b* direction is the most favourable, in a straight line. The barrier site is rather stable, with an intercalation of −2.07 eV. The energy barrier is 0.53 eV. We consider this site being in a plane of four oxygen atoms, with an average Li–O distance of 2.00 Å. And the last path along the [001] direction is with an energy barrier of 0.97 eV. The intercalation site T[001] is in an octahedral environment with Li–O distances of 2.05 Å in average.

3.3.5. Amorphous TiO_2

The energy profile for Li diffusion is visualised in Fig. 3. The same potentials have been successfully used by Yildirim et al. [81] with Molecular Dynamic calculations. The diffusion is anisotropic and leads to some confined regions, which is in agreement with their studies. A detailed analysis of atomistic results will be compared to DFT in another paper.

4. Discussion

The $LiTiO_2$ interatomic potentials that we use for this study, from Kerisit et al. [6], show a good transferability among the titania

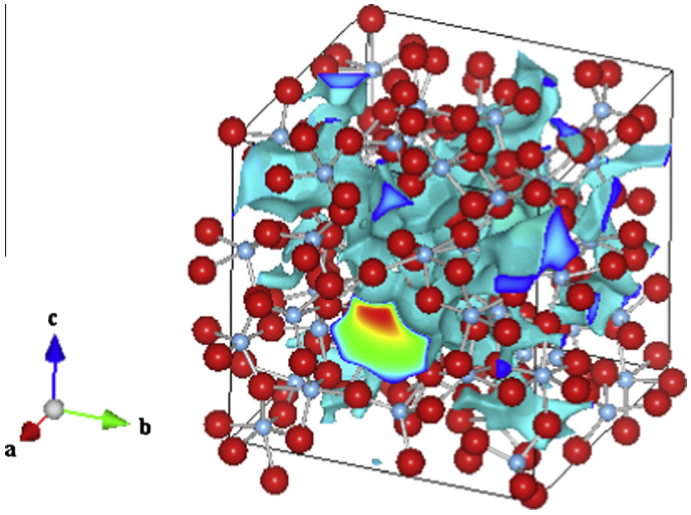

Fig. 3. Pathway for Li-diffusion in amorphous TiO_2 with a density of 3.8 g/cm^3.

polymorphs. We did assume that the reduction process on Ti network and electron hopping is the same within the polymorphs which allow to only take into account the intercalation of Li^+. The energy profile and structural properties for Li migration are consistent with available *ab initio* methods, force-field methods and experimental data as it is shown below.

The most favourable path for each polymorph is along the wider channel. A linear diffusion is expected for rutile along the [001] direction and TiO_2-B along the [010] direction. In brookite, the most favourable path is along the [001] direction. In the latter case, the channels are interconnected by pairs and then the diffusion can occur quasi linearly or in zigzag between the two channels. In the case of TiO_2-B, another channel, thinner, is observed along the [001] direction and it is the second possible path. In anatase, the path for diffusion is in zigzag with equal probability in the three directions of the space. The Li diffusion at low concentration is then anisotropic in the case of rutile, brookite and TiO_2-B whereas it is isotropic in the case of anatase. Those results completely agree with experiments and DFT calculations. Effectively, Johnson [55] did show experimentally an anisotropic diffusion along the *c* direction in rutile, verified with DFT calculations [22] and our channels of diffusion are similar to those obtained from classical MD calculations [83,84]. In the case of anatase, our results also agree with DFT calculations done by Tielens et al. [24] and Koudriachova et al. [15]. We also conclude that Li stays located in octahedral sites with the most stable site being an off-centre site with a long distance Li–O at 3.05 Å which can be neglected in the Li coordination number count (Li being 5-fold). The diffusion between the stable Li site and intermediate site is a zigzag path, as it has been shown by Olson et al. [16] using interatomic potentials with GULP software. Our results are consistent with their observations, we can confirm that the diffusion path is effectively in zigzag but also isotropic along the three directions of the space.

In brookite, Lee et al. [85] did suggest that the diffusion should be along the *c* direction and that is also in agreement with our finding. The lithiated brookite phase seems more difficult to be experimentally characterised due to possible different sites [86] and that can be explained by the fact that the energy profile is wide between two C juxtaposed sites belonging to a different channel. The Li–O distances are between 1.85 and 2.63 Å in the most stable pseudo-octahedral sites.

For TiO_2-B, it was believed by Zukalová et al. [7] that the diffusion occurs along the *b* axis, Arrouvel et al. [4] have later demonstrated using DFT that the most favourable path in TiO_2-B is effectively along the *b* direction and is linear. The second favourable path is along the [001] direction [4]. Those DFT results agree with the present work.

Diffusion paths in all the polymorphs and the main intercalation sites corresponding to stable sites and transition sites (sites at the barrier) refined using GULP are therefore in total agreement with previous experimental and theoretical work. The activation energies have also been calculated for each possible direction and that gives us a direct order on the diffusion coefficients in using the Arrhenius relation.

$$D = D_0 e^{-(E_a/k_B T)}$$

D_0 is the pre-exponential factor, E_a the activation energy, k_B the Boltzmann constant and T the temperature.

Different values have been reported in the literature to deduce the diffusion coefficients or hopping rates from *ab initio* calculations (i.e. a vibrational frequency of 10^{12}/s by Koudriachova et al. [87] and of 10^{13}/s by Tielens et al. [24]).

Considering the lack of data allowing distinguishing the exact frequency within the different polymorphs, we will consider that the D_0 factor or the frequency is the same at low Li concentration and we just report an order of magnitude of the exponential part at 300 and 400 K (see Table 4). We already know from experiments that the diffusion coefficient in rutile can be at least 10^9 faster than in anatase (anatase: $D \sim 10^{-12}$–10^{-17} cm^2/s [26,54], rutile [55]: $D = 2.7 \times 10^{-3}$ cm^2/s along the *c* direction). At 300 K, we calculate a ratio of 2.4×10^6 and this ratio increases as the temperature decreases.

Following the Arrhenius relation, we can see that the temperature influences the diffusion coefficient/hopping rate. We can also evaluate the temperature needed to obtain the same mobility for a direction of diffusion in a polymorph. For example, if we want to increase the mobility along the [001] direction of TiO_2-B in order to get the same performance of the [010] direction at 300 K, we solve:

$$\frac{E_{a1}}{T_1} = \frac{E_{a2}}{T_2}$$

So for T_1 = 300 K, E_{a1} = 0.53 eV and E_{a2} = 0.97 eV, that induces a temperature T_2 of 549 K.

The temperature will have therefore a strong influence on experimental measurement and on the mobility of the lithium. We also note that the hopping distance in rutile is the shortest (at 1.50 Å along *c* direction) while in TiO_2-B, the hopping distance

Table 4
Hopping distances, activation energies and exponential factor in Arrhenius relation at 300 K and 400 K for the main directions along TiO_2 polymorphs.

Polymorph	Direction	Hopping distance (Å)	E_{act}[a] (eV)	E_{act}[b] (eV)	E_{act}[c] (eV)	$e^{-(E_a/k_BT)}$ at T = 300 K[a]	$e^{-(E_a/k_BT)}$ at T = 400 K[a]
Rutile	[001]	1.50	**0.04**	0.04 [87]	0.3 [55]	0.2128	0.3133
	[110]	3.26	1.91	0.8 [87]		8.2×10^{-33}	8.6×10^{-25}
Anatase	[201]	3.03	**0.42**	0.6 [16]; 1.3 [24]	0.5 [26]	8.8×10^{-08}	5.11×10^{-06}
Brookite	[001]	2.95	**1.07**	–	–	1.1×10^{-18}	3.3×10^{-14}
TiO_2-B	[100]	6.72	1.09	0.9 [4]		4.9×10^{-19}	1.8×10^{-14}
	[010]	3.76	**0.53**	0.3 [4]	0.4 [56]	1.2×10^{-09}	2.1×10^{-07}
	[001]	7.14	0.97	0.5 [4]		5.1×10^{-17}	6.0×10^{-13}

Activation energy.
[a] Our work (in bold, lowest activation energy).
[b] Other theoretical work.
[c] Experimental work.

is the longest (3.76 Å along *b* direction). The frequency to jump from one site to the other is therefore higher on rutile.

In general, the calculated order for the diffusion coefficient at a given temperature and in neglecting any concentration and hopping distance effects is:

$$\text{rutile } [001] > \text{anatase } [201] > TiO_2\text{-B } [010] > TiO_2\text{-B } [001] > TiO_2\text{-B } [100] \sim \text{brookite } [001] > \text{rutile } [110]$$

We can then demonstrate that the temperature has a clear effect on the coefficient diffusion and on direction of diffusion which is in agreement with experimental data. In the case of the anatase, it has been experimentally shown that with the increase of the temperature (at 250 K), the diffusion increases as well [26]. At low temperature, the most favourable direction for the diffusion should be with the lowest energy profile and an increase of the temperature will facilitate the diffusion along the other anisotropic directions. This is in agreement with the observations made by Koudriachova et al. [87] who did interpret the change of direction in rutile from lower temperatures along the *c* direction to higher temperatures along the *a*–*b* plane.

However, one of the key factors to insert Li within the bulk is to give to the system enough energy to cross the energy barriers for the ion diffusion, and then the intercalation energy of the transition site will be an important factor. The influence of the geometry of the transition sites is significant on the intercalation energy. We can generalise some concepts which have already been mentioned by different authors [24], the Oh sites are energetically more stable than the Td sites, as the distances are longer in an Oh environment. Also, the transition sites are not visible experimentally; NMR studies can deduce the coordination number of the stable sites and evaluate the activation energy of the Li diffusion. It was often reported that Li is located in an octahedral site in anatase [25,26,28] and it is 4-fold, while it was believed that Li is in the squared pyramid and is 5-fold [36,88] in TiO_2-B. At low Li concentration, we find that the Li is 5-fold in an Oh site while the stable off-C site is 4 or 6-fold in TiO_2-B. Our study agrees with previous theoretical work at low concentration [4,15,24] and it has also been shown that the Li concentration has an effect on the Li position [3,6,89].

Based on a wide range of theoretical and experimental studies on the insertion of Li on TiO_2 polymorphs and amorphous phases [27,29,32,39,40,49,55,81,90–92], our simulations help to rationalise the geometry of the intercalation sites and the energetic governing the mobility of Li in the bulk.

This method including a 3D scan for Li diffusion will be therefore worthwhile to further extend in generalising to the diffusion of intrinsic and extrinsic defects to a wide range of other materials from crystalline to amorphous phases.

5. Conclusion

Through a 3D scan of the Li migration and energy defect calculations, energy minimisation techniques can give a clear description of paths for ion diffusion in oxides. The existence of channels has already been evidenced using other techniques, such as classical Molecular Dynamics in the rutile phase [83] and we have generalised the work to the other polymorphs. Our results also agree with previous experimental and theoretical data on activation energies and directions of diffusion in rutile and TiO_2-B, having both a clear anisotropic behaviour. We can show that the anatase has, at the opposite, an isotropic diffusion at low Li concentration. The brookite phase, being less known, shows an anisotropic diffusion along the *c*-axis with unfavourable energy barriers. Pairs of channels are linked by a small canal with different intercalation sites. The diffuse energy profile and low symmetry of Li sites explain why the Li-brookite phase is more difficult to characterise experimentally with XDR techniques, the intercalation being more difficult and more localised in the segment linking the channels.

The activation energy order of each polymorph predicts the order of the diffusion coefficients. The order is as follows:

$$\text{rutile } [001] > \text{anatase } [201] > TiO_2\text{-B } [010] > TiO_2\text{-B } [001] > TiO_2\text{-B } [100] \sim \text{brookite } [001] > \text{rutile } [110]$$

The highest diffusion coefficient is observed in rutile but it does not reflect the potentiality of the material. In fact, it should be combined with the intercalation energy of each sites, the number of neighbour sites and the hopping distances. We have shown that the intercalation energy depends on the environment of each site. An octahedral site is more favourable than a tetrahedral site which can simply be explained by distance criterions (Oh site having longer Li–O distances compared to Td site). The environment of each calculated site can be compared to available NMR and XRD experimental data and that agrees with previous studies.

The anatase has the advantage to have an isotropic diffusion between octahedral sites and can compete with TiO_2-B. To improve the potentiality of an anisotropic material such as TiO_2-B, we suggest that the shape of nanoparticles should be a crucial factor. In that sense, the TiO_2-B particle should better have an open access to the infinite channel along the *b*-axis, which can be possible with the existence of exposed (010) and (110) surfaces.

A simple approach based on scanning the Li positions with interatomic potentials gives a reliable description of the pathways for Lithium diffusion and represents a powerful complementary approach for studying the migration of ions in the bulk and at the interfaces of oxides.

Future work will consider electronic properties of the selected intercalated sites, particularly in the brookite and amorphous phases.

Acknowledgements

The authors would like to thank FAPITEC and CNPq for financial support and for providing a PIBIC fellowship. CA acknowledges CENAPAD-SP Campinas for computational resources (project number 554).

References

[1] J.-M. Tarascon, Key challenges in future Li-battery research, Phil. Trans. Roy. Soc. 368 (2010) 3227–3241.
[2] M.S. Islam, Recent atomistic modelling studies of energy materials: batteries included, Phil. Trans. Roy. Soc. 368 (2010) 3255–3267.
[3] A.R. Armstrong, V. Gentili, P.G. Bruce, C. Arrouvel, S.C. Parker, M.S. Islam, Lithium coordination sites in LixTiO$_2$(B): a structural and computational study, Chem. Mater. 22 (2010) 6426–6432.
[4] C. Arrouvel, S.C. Parker, M.S. Islam, Lithium insertion and transport in the TiO$_2$-B anode material: a computational study, Chem. Mater. 21 (2009) 4778–4783.
[5] D. Panduwinata, J.D. Gale, A first principles investigation of lithium intercalation in TiO$_2$-B, J. Mater. Chem. 19 (2009) 3931–3940.
[6] S. Kerisit, K.M. Rosso, Z. Yang, J. Liu, Computer Simulation of the phase stabilities of lithiated TiO$_2$ polymorphs, J. Phys. Chem. C 114 (2010) 19096–19107.
[7] M. Zukalová, M. Kalbác, L. Kavan, I. Exnar, M. Graetzel, Pseudocapacitive lithium storage in TiO$_2$(B), Chem. Mater. 17 (2005) 1248–1255.
[8] G. Armstrong, A.R. Armstrong, J. Canales, P.G. Bruce, TiO$_2$(B) nanotubes as negative electrodes for rechargeable lithium batteries, Electrochem. Solid-State Lett. 9 (2006) A139–A143.
[9] P.G. Bruce, Energy materials, Solid State Sci. 7 (2005) 1456–1463.
[10] Q. Li, J. Zhang, B. Liu, M. Li, S. Yu, L. Wang, Z. Li, D. Liu, Y. Hou, Y. Zou, B. Zou, T. Cui, G. Zou, Synthesis and electrochemical properties of TiO$_2$-B@C core-shell nanoribbons, Cryst. Growth Des. 8 (2008) 1812–1814.
[11] T.P. Feist, P.K. Davies, The soft chemical synthesis of TiO$_2$(B) from layered titanates, J. Solid State Chem. 101 (1992) 275–295.
[12] J.F. Banfield, D.R. Veblen, D.J. Smith, The identification of naturally occurring TiO$_2$(B) by structure determination using high-resolution electron microscopy. Image simulation, and distance-least-squares refinement, Am. Miner. 76 (1991) 343–353.
[13] F. Schossberger, Uber die Umwandlung des Titandioxyds, Z. Kristallogr. Krist. 104 (1942) 358.
[14] M. Pauling, J.-H. Sturdivant, The crystal structure of brookite, Z. Kristallogr. Kristallogeom. Kristallophys. Kristallochem. 68 (1928) 239–256.
[15] M.V. Koudriachova, S.W. de Leeuw, N.M. Harrison, Orthorhombic distortion on Li intercalation in anatase, Phys. Rev. B 69 (2004) 54106.
[16] C.L. Olson, J. Nelson, M.S. Islam, Defect chemistry, surface structures, and lithium insertion in anatase TiO$_2$, J. Phys. Chem. B 110 (2006) 9995–10001.
[17] R. Baddour-Hadjean, S. Bach, M. Smirnov, J.-P. Pereira-Ramos, Raman investigation of the structural changes in anatase Li$_x$TiO$_2$ upon electrochemical lithium insertion, J. Raman Spectrosc. 35 (2004) 577–585.
[18] W.C. Mackrodt, First principles Hartree-Fock description of lithium insertion in oxides I. The end members TiO$_2$ and LiTiO$_2$ of the system Li$_x$TiO$_2$, J. Solid State Chem. 142 (1999) 428–439.
[19] S. Lunell, A. Stashans, L. Ojamäe, H. Lindström, A. Hagfeldt, Li and Na diffusion in TiO$_2$ from quantum chemical theory versus electrochemical experiment, J. Am. Chem. Soc. 119 (1997) 7374–7380.
[20] A. Stashans, S. Lunell, R. Bergström, A. Hagfeldt, S.-T. Lindquist, Theoretical study of lithium intercalation in rutile and anatase, Phys. Rev. B 53 (1996) 159–170.
[21] M.V. Koudriachova, N.M. Harrison, S.W. de Leeuw, First principles predictions for intercalation behaviour, Solid State Ionics 175 (2004) 829–834.
[22] M.V. Koudriachova, N.M. Harrison, S.W. de Leeuw, Diffusion of Li-ions in rutile. An ab initio study, Solid State Ionics 157 (2003) 35–38.
[23] G. Nuspl, K. Yoshizawa, T. Yamabe, Lithium intercalation in TiO$_2$ modifications, J. Mater. Chem. 7 (1997) 2529–2536.
[24] F. Tielens, M. Calatayud, A. Beltrán, C. Minot, J. Andrés, Lithium insertion and mobility in the TiO$_2$-anatase/titanate structure: a periodic DFT study, J. Electroanal. Chem. 581 (2005) 216–223.
[25] M. Wagemaker, G.J. Kearley, A.A. van Well, H. Mutka, F.M. Mulder, Multiple Li positions inside oxygen octahedra in lithiated TiO$_2$ anatase, J. Am. Chem. Soc. 125 (2003) 840–848.
[26] M. Wagemaker, R. van de Krol, A.P.M. Kentgens, A.A. van Well, F.M. Mulder, Two phase morphology limits lithium diffusion in TiO$_2$ (anatase): a Li-7 MAS NMR study, J. Am. Chem. Soc. 123 (2001) 11454–11461.
[27] M. Wagemaker, D. Lützenkirchen-Hecht, A.A. van Well, R. Frahm, Atomic and electronic bulk versus surface structure: lithium intercalation in anatase TiO$_2$, J. Phys. Chem. B 108 (2004) 12456–12464.
[28] D.W. Murphy, M. Greenblatt, S.M. Zahurak, R.J. Cava, J.V. Waszczak, G.W. Hull, R.S. Hutton, Lithium insertion in anatase – a new route to the spinel LiTi2O4, Rev. Chim. Miner. 19 (1982) 441–449.
[29] S. Södergren, H. Siegbahn, H. Rensmo, H. Lindström, A. Hagfeldt, S.-T. Lindquist, Lithium intercalation in nanoporous anatase TiO$_2$ studied with XPS, J. Phys. Chem. B 101 (1997) 3087–3090.
[30] T. Ohzuku, T. Kodama, T. Hirai, Electrochemistry of anatase titanium dioxide in lithium nonaqueous cells, J. Power Sour. 14 (1985) 153–166.
[31] R.J. Cava, D.W. Murphy, S.M. Zahurak, A. Santoro, R.S. Roth, The crystal structures of the lithium-inserted metal oxides Li$_{0.5}$TiO$_2$ anatase, LiTi$_2$O$_4$ spinel, and Li$_2$Ti$_2$O$_4$, J. Solid State Chem. 53 (1984) 64–75.
[32] B. Zachau-Christiansen, K. West, T. Jacobsen, S. Atlung, Lithium insertion in different TiO$_2$ modifications, Solid State Ion. 28–30 (1988) 1176–1182.
[33] M.A. Reddy, U.V. Varadaraju, Lithium insertion in micrometer sized rutile TiO$_2$ at room temperature: facilitated by crystal chemical substitution, J. Electrochem. Soc. 161 (2014) A149–A153.
[34] C.R.A. Catlow, A.N. Cormack, F. Theobald, Structure prediction of transition-metal oxides using energy-minimization techniques, Acta Cryst. B40 (1984) 195–200.
[35] V. Swamy, J.D. Gale, L.S. Dubrovinsky, Atomistic simulation of the crystal structures and bulk moduli of TiO$_2$ polymorphs, J. Phys. Chem. Solids 62 (2001) 887–895.
[36] L. Brohan, R. Marchand, Physical Properties of Bronze MxTiO$_2$(B), Solid State Ionics 9/10 (1983) 419.
[37] A.G. Dylla, G. Henkelman, K.J. Stevenson, Lithium insertion in nanostructured TiO$_2$(B) architectures, Acc. Chem. Res. 46 (2013) 1104–1112.
[38] M. Fehse, M. Ben Yahia, L. Monconduit, F. Lemoigno, M.L. Doublet, F. Fischer, C. Tessier, L. Stievano, New insights on the reversible lithiation mechanism of TiO$_2$(B) by Operando X-ray absorption spectroscopy and X-ray diffraction assisted by first-principles calculations, J. Phys. Chem. C 118 (2014) 27210–27218.
[39] L.D. Noailles, C.S. Johnson, J.T. Vaughey, M.M. Thackeray, Lithium insertion into hollandite-type TiO$_2$, J. Power Sour. 81–82 (1999) 259–263.
[40] J. Akimoto, Y. Gotoh, M. Sohma, K. Kawaguchi, Y. Oosawa, H. Takei, Synthesis and crystal structure of Ramsdellite-type Li$_{0.5}$TiO$_2$, J. Solid State Chem. 110 (1994) 150–155.
[41] K.M. Colbow, J.R. Dahn, R.R. Haering, Structure and electrochemistry of the spinel oxides LiTi$_2$O4 and Li$_4$/3Ti5/3O4, J. Power Sour. 26 (1989) 397–402.
[42] M. Sakao, N. Kijima, J. Akimoto, T. Okutani, Lithium insertion and extraction properties of hollandite-type K$_x$TiO$_2$ with different K content in the tunnel space, Solid State Ionics 243 (2013) 22–29.
[43] Y.H. Liu, J.Y. Wu, W. Zhao, J.L. Chu, T. Qi, Study on lithium insertion in lepidocrocite and lambda-MnO$_2$ type TiO$_2$: a first-principles prediction, Chin. J. Chem. 31 (2013) 1257–1262.
[44] M.A. Reddy, V. Pralong, U.V. Varadaraju, B. Raveau, Crystallite size constraints on lithium insertion into brookite TiO(2), Electrochem. Solid-State Lett. 11 (2008) A132–A134.
[45] M.A. Reddy, M.S. Kishore, V. Pralong, U.V. Varadaraju, B. Raveau, Electrochem. Solid-State Lett. 10 (2001) A29.
[46] D.W. Murphy, R.J. Cava, S.M. Zahurak, A. Santoro, Ternary Li$_x$TiO$_2$ phases from insertion reactions, Solid State Ionics 9–10 (1983) 413–417.
[47] M.J. Sussman, M. Celikin, A. Yasin, G.P. Demopoulos, Mesoporous brookite nanoplatelets with superior lithium-ion intercalation stability, Electrochim. Acta 138 (2014) 215–223.
[48] Y.C. Jiao, F. Chen, L.Q. Zhang, E.L. Zhou, J.L. Zhang, Hydrothermal synthesis of anatase and brookite nanotubes with superior photocatalytic and Li+ insertion/extraction performances, Catal. Commun. 47 (2014) 32–35.
[49] W.J.H. Borghols, D. Lützenkirchen-Hecht, U. Haake, W. Chan, U. Lafont, E.M. Kelder, E.R.H. van Eck, A.P.M. Kentgens, F.M. Mulder, M. Wagemakera, Lithium storage in amorphous TiO$_2$ nanoparticles, J. Electrochem. Soc. 157 (2010) A582–A588.
[50] D. Guan, C. Cai, Y. Wang, Amorphous and crystalline TiO$_2$ nanotube arrays for enhanced Li-ion intercalation properties, J. Nanosci. Nanotechnol. 11 (2011) 3641–3650.
[51] E. Baudrin, S. Cassaignon, M. Koelsh, J.-P. Jolivet, L. Dupont, J.-M. Tarascon, Structural evolution during the reaction of Li with nano-sized rutile type TiO$_2$ at room temperature, Electrochem. Commun. 9 (2007) 337–342.
[52] W.J. Macklin, R.J. Neat, Performance of titanium dioxide-based cathodes in a lithium polymer electrolyte cell, Solid State Ion. 53–56 (1992) 694–700.
[53] P. Bottke, Y. Ren, I. Hanzu, P.G. Bruce, M. Wilkening, Li ion dynamics in TiO$_2$ anode materials with an ordered hierarchical pore structure – insights from ex situ NMR, Phys. Chem. Chem. Phys. 16 (2014) 1894–1901.
[54] Z. Liu, L. Hong, B. Guo, Physicochemical and electrochemical characterization of anatase titanium dioxide nanoparticles, J. Power Sour. 143 (2005) 231–235.
[55] O.W. Johnson, One-dimensional diffusion of Li in rutile, Phys. Rev. A 136 (1964) A284–A290.
[56] M. Wilkening, C. Lyness, A.R. Armstrong, P.G. Bruce, Diffusion in confined dimensions: Li+ transport in mixed conducting TiO$_2$-B nanowires, J. Phys. Chem. C 113 (2009) 4741–4744.
[57] G.W. Watson, E.T. Kelsey, N.H. de Leeuw, D.J. Harris, S.C. Parker, Atomistic simulation of dislocations, surfaces and interfaces in MgO, J. Chem. Soc. Faraday Trans. 92 (1996) 433–438.
[58] J.D. Gale, A.L. Rohl, The general utility lattice program (GULP), Mol. Simul. 29 (2003) 291–341.
[59] J.D. Gale, Semi-empirical methods as a tool in solid-state chemistry, J. Chem. Soc., Faraday Trans. 93 (1997) 629–632.

[60] M. Born, K. Huang, Dynamical Theory of Crystal Lattices, New York, 1954.
[61] M. Matsui, M. Akoagi, Mol. Simul. 6 (1991) 239.
[62] K. Momma, F. Izumi, VESTA: a three-dimensional visualization system for electronic and structural analysis, J. Appl. Crystallogr. 41 (2008) 653–658.
[63] N.F. Mott, M.J. Littleton, Conduction in polar crystals. I. Electrolytic conduction in solid salts, Trans. Faraday Soc. 34 (1938) 485–499.
[64] X. Bokhimi, A. Morales, F. Pedraza, Crystallography and crystallite morphology of rutile synthesized at low temperature, J. Solid State Chem. 169 (2002) 176–181.
[65] J.K. Burdett, T. Hughbanks, G.J. Miller, J.W.J. Richardson, J.V. Smith, Structural-electronic relationships in inorganic solids: powder neutron diffraction studies of the rutile and anatase polymorphs of titanium dioxide at 15 and 295 K, J. Am. Chem. Soc. 109 (1987) 3639–3646.
[66] W.H. Baur, Atomabstaende und Bindungswinkel im Brookit, TiO_2, Z. Kristallogr. Kristallogeom. Kristallophys. Kristallochem. 111 (1959) 401–420.
[67] Q. Li, B. Liu, L. Wang, D. Li, R. Liu, B. Zou, T. Cui, G. Zou, Pressure-induced amorphization and Polyamorphism in one-dimensional single-crystal TiO_2 nanomaterials, J. Phys. Chem. Lett. 1 (2010) 309–314.
[68] V. Petkov, G. Holzhüter, U. Tröge, T. Gerber, B. Himmel, Atomic-scale structure of amorphous TiO_2 by electron, X-ray diffraction and reverse Monte Carlo simulations, J. Non-Cryst. Solids 231 (1998) 17–30.
[69] S.O. Kucheyev, T. van Buuren, T.F. Baumann, J.H. Satcher Jr., T.M. Willey, R.W. Meuleberg, T.E. Felter, J.F. Poco, S.A. Gammon, L.J. Terminello, Electronic structure of titania aerogels from soft X-ray absorption spectroscopy, Phys. Rev. B 69 (2004) 245102.
[70] D. Mergel, D. Buschendorf, S. Eggert, R. Grammes, B. Samset, Density and refractive index of TiO_2 films prepared by reactive evaporation, Thin Solid Films 371 (2000) 218–224.
[71] V. Swamy, A. Kuznetsov, L.S. Dubrovinsky, P.F. McMillan, V.B. Prakapenka, G. Shen, B.C. Muddle, Size-dependent pressure-induced amorphization in nanoscale TiO_2, Phys. Rev. Lett. 96 (2006) 135702.
[72] I. Manzini, G. Antonioli, D. Bersani, P.P. Lottici, G. Gnappi, A. Montenero, X-ray absorption spectroscopy study of crystallization processes in sol–gel-derived TiO_2, J. Non-Cryst. Solids 193 (1995) 519–523.
[73] R. Lizárraga, E. Holmström, S.C. Parker, C. Arrouvel, Structural characterization of amorphous alumina and its polymorphs from first-principles XPS and NMR calculations, Phys. Rev. B 83 (2011) 094201.
[74] G. Kresse, J. Hafner, Ab initio molecular-dynamics simulation of the liquid-metal–amorphous-semiconductor transition in germanium, Phys. Rev. B 49 (1994) 14251–14269.
[75] J.P. Perdew, Y. Wang, Accurate and simple analytic representation of the electron-gas correlation energy, Phys. Rev. B 45 (1992) 13244–13249.
[76] G. Kresse, D. Joubert, From ultrasoft pseudopotentials to the projector augmented-wave method, Phys. Rev. B 59 (1999) 1758–1775.
[77] J.-P. Rino, N. Studart, Structural correlations in titanium dioxide, Phys. Rev. B 59 (1999) 6643–6649.
[78] H. Zhang, B. Chen, J.B. Banfield, Atomic structure of nanometer-sized amorphous TiO_2, Phys. Rev. B 78 (2008) 214106.
[79] I. Hotovy, V. Rehacek, P. Siciliano, S. Capone, L. Spiess, Sensing characteristics of NiO thin films as NO_2 gas sensor, Thin Solid Films 418 (2002) 9–15.
[80] V.V. Hoang, H. Zung, N.H.B. Trong, Structural properties of amorphous TiO_2 nanoparticles, Eur. Phys. J. D 44 (2007) 515–524.
[81] H. Yildirim, J.P. Greeley, S. Sankaranarayanan, Localized order–disorder transitions induced by Li segregation in amorphous TiO_2 nanoparticles, ACS Appl. Mater. Interfaces 6 (2014) 18962–18970.
[82] V.V. Hoang, The glass transition and diffusion in simulated liquid TiO_2, J. Phys. D: Appl. Phys. 40 (2007) 7454.
[83] F. Gligor, S.W. de Leeuw, Solid State Ionics 177 (2006) 2741.
[84] H. Yildirim, J.P. Greeley, S.K.R.S. Sankaranarayanan, The effect of concentration on Li diffusivity and conductivity in rutile TiO_2, Phys. Chem. Chem. Phys. 14 (2012) 4565–4576.
[85] D.-H. Lee, J.-G. Park, K.J. Choi, H.-J. Choi, D.-W. Kim, Preparation of brookite-type TiO_2/carbon nanocomposite electrodes for application to Li ion batteries, Eur. J. Inorg. Chem. 6 (2008) 878–882.
[86] M.A. Reddy, M.S. Kishore, V. Pralong, U.V. Varadaraju, B. Raveau, Lithium intercalation into nanocrystalline brookite TiO_2, Electrochem. Solid-State Lett. 10 (2007) A29–A31.
[87] M.V. Koudriachova, N.M. Harrison, S.W. de Leeuw, Effect of diffusion on lithium intercalation in titanium dioxide, Phys. Rev. Lett. 86 (2001) 1275–1278.
[88] M. Tournoux, R. Marchand, L. Brohan, Layered $K_2Ti_4O_9$ and the open metastables TiO_2(B) structure, Prog. Solid State Chem. 17 (1986) 33–52.
[89] M.V. Koudriachova, N.M. Harrison, S.W. de Leeuw, Structural deformations in lithium doped titanium dioxide, Comp. Mater. Sci. 24 (2002) 235–240.
[90] D. Bi, J. Wang, Y. Sun, Z. Liao, Proc. Electrochem. Soc. 80 (1980) 245.
[91] R.K.B. Gover, J.R. Tolchard, H. Tukamoto, T. Murai, J.T.S. Irvine, J. Electrochem. Soc. 146 (1999) 4348.
[92] J. Akimoto, Y. Gotoh, Y. Oosawa, N. Nonose, T. Kumagai, K. Aoki, H. Takei, Topotactic oxidation of Ramsdellite-type $Li_{0.5}TiO_2$, a new polymorph of titanium dioxide: TiO_2(R), J. Solid State Chem. 113 (1994) 27–36.